Digestive Ripening of Thiolated Gold Nanoparticles: The Effect of Alkyl Chain Length

B. L. V. Prasad,† Savka I. Stoeva,† Christopher M. Sorensen,*,‡ and Kenneth J. Klabunde*,†

Department of Chemistry, and Department of Physics, Kansas State University, Manhattan, Kansas 66506

Received February 19, 2002. In Final Form: July 1, 2002

Digestive ripening, heating a colloidal suspension at or near the solvent boiling point in the presence of a surface-active ligand, was applied to polydisperse colloidal gold in toluene using a series of alkylthiols, viz., octyl-, decyl-, dodecyl-, and hexadecylthiols. In all the instances, digestive ripening significantly reduced the average particle size and polydispersity. All the colloids remain suspended in solution above 80 °C, but at room temperature the tendency to form 3D superlattices and precipitate increased with declining alkyl chain length. For example, using octanethiol as the ligand makes the colloids aggregate into big 3D superlattices and precipitate; decane- and dodecanethiol also produce precipitated 3D superlattices along with separate particles, while hexadecanethiol-coated particles remain well separated from each other. The optical spectra at room temperature reveal, apart from the gold plasmon band at 530 nm, a large tail above 700 nm for Au−octanethiol and Au−decanethiol cases and a shoulder at 630 nm for Au−dodecanethiol attributed to the superlattices. Au−hexadecanethiol, on the other hand, shows only the gold plasmon band as expected from separate particles. However, at higher temperatures only the gold plasmon band is observed for all the colloids indicating the dissolution of the superlattices. The aggregation of the particles into 3D superlattices or their stability as a colloidal suspension is qualitatively explained on the basis of decreasing van der Waals attraction between the gold nanoparticles as the separation between them is increased through the alkyl chain length of the capping ligand from octyl to hexadecyl.

Introduction

Preparation of highly monodisperse gold nanoparticles through different techniques is still attracting significant interest,[1] and several methods have been successfully developed and tested.[2] Reducing metal salts in the presence of a surfactant and arresting the size of the as-prepared metal particle by a capping ligand, already present in the solution, is the most general method employed for the synthesis of monodisperse colloidal particles.[2a] The size, shape, and interparticle separation of these uniform size distributed particles are crucially controlled by the nature of the capping ligands.[3] The most popular ligands for capping gold nanoparticles are the alkanethiols[2,3] or some modified thiols.[4]

Recently, some of us have reported the effectiveness of an alternate route to monodisperse colloidal gold, the digestive ripening method. This method converts a polydisperse colloidal suspension into a highly monodisperse one.[5] It involves the refluxing of gold nanoparticles in the presence of an excess capping ligand and transforms even an extremely polydisperse colloid into a highly monodisperse one. This procedure is particularly advantageous in large-scale syntheses where polydisperse nanoscale gold particles are formed. The applicability of this method for large-scale synthesis of gold−dodecanethiol nanoparticles and their arrangement in large superlattices has also been demonstrated.[6] Our previous work used 1-dodecanethiol ($C_{12}H_{25}SH$) as the ligand.[5,6] The purpose of this paper is to evaluate the efficacy of this method with ligands such as 1-octanethiol ($C_8H_{17}SH$), 1-decanethiol ($C_{10}H_{21}SH$), and 1-hexadecanethiol ($C_{16}H_{33}SH$) and describe the resulting colloids and superlattices for gold nanoparticles. We find that all these ligands function as digestive ripening agents. The gold nanoparticles produced in each case are highly monodisperse and show a small increase in the mean size with increasing alkyl chain length. They display different solubilities as a function of temperature seen qualitatively through precipitation of superlattices and UV−vis spectroscopy. These solubility differences affect the 2D or 3D superlattice formation when the colloidal solutions are cooled or when evaporated on transmission electron microscopy (TEM) grids. UV−vis spectroscopy also shows an unusual red shift of the plasmon absorption for Au−octanethiol and Au−decanethiol superlattices. Both the solubility differences and the optical absorption spectra of these aggregates are ascribed to the closest interparticle separation allowed by the different ligands.

* Corresponding authors. E-mail: kenjk@ksu.edu, sor@phys.ksu.edu. Phone: (785)-532-6849. Fax: (785)-532-6666.

† Department of Chemistry.

‡ Department of Physics.

(1) (a) Lin, J.; Zhou, W.; O'Connor, C. J. *Mater. Lett.* **2001**, *49*, 282. (b) Zhou, Y.; Itoh, H.; Uemura, T.; Naka, K.; Chujo, Y. *Langmuir* **2002**, *18*, 277. (c) Weare, W. W.; Reed, S. M.; Warner, M. G.; Hutchson, J. E. *J. Am. Chem. Soc.* **2000**, *122*, 12890.

(2) (a) Brust, M.; Walker, M.; Bethell, D.; Schiffrin, D. J.; Whyman, R. *J. Chem. Soc., Chem. Commun.* **1994**, 801. (b) Andres, R. P.; Bielfeld, J. D.; Henderson, J. I.; Janes, D. B.; Kolagunta, V. R.; Kubiak, C. P.; Mahoney, W. J.; Osifchin, R. G. *Science* **1995**, *273*, 1690. (c) Spatz, J. P.; Roescher, A.; Moleller, M. *Adv. Mater.* **1996**, *8*, 337.

(3) (a) Hostetler, M. J.; Wingate, J. E.; Zhong, C. J.; Harris, J. E.; Vachet, R. W.; Clark, M. R.; Londono, J. D.; Green, S. J.; Stokes, J. J.; Wignall, G. D.; Glish, G. L.; Porter, M. D.; Evans, N. D.; Murray, R. W. *Langmuir* **1998**, *14*, 17. (b) Martin, J. E.; Wilcoxon, J. P.; Odinek, J.; Provencio, P. *J. Phys. Chem. B* **2000**, *104*, 9475. (c) Heath, J. R.; Knobler, C. M.; Leff, D. V. *J. Phys. Chem. B* **1997**, *101*, 189. (d) Weare, W. W.; Reed, S. M.; Warner, M. G.; Hutchison, J. E. *J. Am. Chem. Soc.* **2000**, *122*, 12890.

(4) Kim, B.; Tripp, S. L.; Wei, A. *J. Am. Chem. Soc.* **2001**, *123*, 7955.

(5) (a) Lin, X. M.; Sorensen, C. M.; Klabunde, K. J. *J. Nanopart. Res.* **2000**, *2*, 154. (b) Lin, X. M.; Wang, G. M.; Sorensen, C. M.; Klabunde, K. J. *J. Phys. Chem. B* **1999**, *103*, 5488. (c) Lin, X. M.; Jaeger, H. M.; Sorensen, C. M.; Klabunde, K. J. *J. Phys. Chem. B* **2001**, *105*, 3353.

(6) Stoeva, S. I.; Klabunde, K. J.; Sorensen, C. M.; Dragieva, I. *J. Am. Chem. Soc.* **2002**, *124*, 2305.

10.1021/la020181d CCC: $22.00
Published on Web 08/29/2002

Experimental Procedures

The sample preparation was carried out following already published procedures,[5] and hence only a brief description is given here. All the reactions were carried out in a closed Ar atmosphere, and all the solvents were dried and degassed by bubbling dry Ar gas for 4 h prior to use. In a typical experiment, a 0.02 M micelle solution of dodecyldimethylammonium bromide (DDAB) was prepared in 10 mL of toluene. $AuCl_3$ (34 mg) was then dissolved in this micelle solution by sonication to form a dark orange solution. Aqueous $NaBH_4$ solution (36 μL, 9.4 M) was then added dropwise to this gold chloride−micelle solution while vigorously stirring. The dark orange solution turned red within a minute, and the stirring was continued for at least 15 min to make sure the reaction was complete.

The "as-prepared" gold colloid thus formed was then split into 2.5 mL portions. Alkanethiol was added to each portion keeping the molar ratio of Au/thiol at 1:30. We have used 1-octanethiol ($C_8H_{17}SH$), 1-decanethiol ($C_{10}H_{21}SH$), 1-dodecanethiol ($C_{12}H_{25}SH$), and 1-hexadecanethiol ($C_{16}H_{33}SH$) in this study. The alkanethiol-coated gold particles were then separated from the DDAB, excess thiol, and the reaction side products by precipitating with 7.5 mL of ethanol. The particles which settled down to the bottom of the sample vial were isolated from the supernatant by decanting and vacuum-drying. The gold particles were then redispersed in 2.5 mL of toluene. For digestive ripening, another dose of the respective thiols with the same molar ratio (Au/thiol = 1:30) was added to the sample and then refluxed under an Ar atmosphere for 90 min. The colloids were then transferred into sample vials and were allowed cool to room temperature. Portions (3 μL) of these colloids were then taken on to a carbon-coated Formvar copper grid for TEM imaging after vigorously shaking the sample vials. The colloids digestive-ripened by $C_8H_{17}SH$, $C_{10}H_{21}SH$, $C_{12}H_{25}SH$, and $C_{16}H_{33}SH$ are designated as Au−C_8SH, Au−C_{10}SH, Au−C_{12}SH, and Au−C_{16}SH, respectively, to facilitate discussion.

TEM images were taken with a Phillips EM100 microscope operating at 100 kV. The particle size distributions were determined from a sample of a minimum of 300 particles. UV−vis spectra were taken on a Spectral Instruments 400 series spectrophotometer, and toluene was the solvent used. Temperature-controlled experiments were performed using a water bath.

Results and Discussion

Somewhat monodisperse colloidal particles can be synthesized by carefully controlling the amounts of surfactant and water, the rate of the reaction, and the reaction temperature. Here, the sizes of the nanoparticles are generally controlled by the surfactants used to form the micellar solutions. However, the resulting colloids are usually characterized by some broad size distributions due to the inherent instability of the micelles in the dynamical synthetic environment. Narrowing the size distribution is often achieved by slow precipitation based on the size-dependent solubility of colloidal particles in a solvent or solvent mixtures.[7] This is a very tedious process since the solubilities of particles with similar sizes are not much different. Therefore, the digestive ripening method which can transform a highly polydisperse colloid into a uniform size distributed one becomes extremely useful.[5] In our synthetic procedure, we purposefully prepared a highly polydisperse gold colloid by using lower concentrations of the surfactant[8] for two reasons. First, it was necessary to remove the surfactant before the digestive ripening step and a smaller amount of the surfactant would be easier to remove, and second, we wanted to confirm the efficacy of digestive ripening with different alkanethiols, which was earlier reported with dodecanethiol.[5,6] The vastly polydisperse colloids thus prepared are depicted in Figure 1. The shapes of the colloids are typically polyhedral.

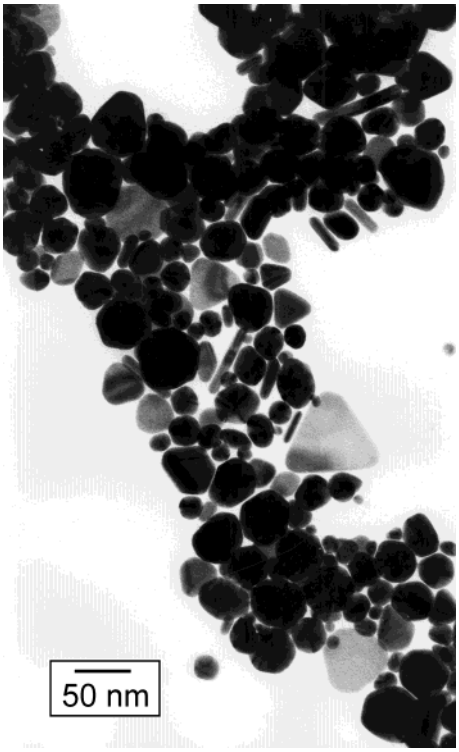

Figure 1. TEM image of the as-prepared colloid. Note the polyhedral structure of the particles and the few thin prisms present.

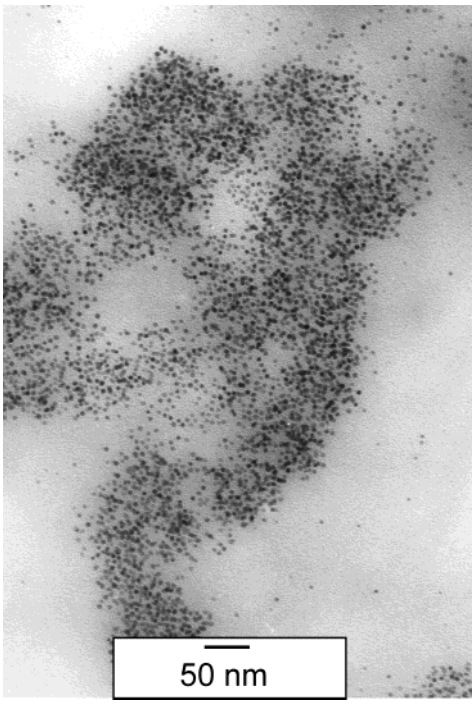

Figure 2. TEM image of the gold colloid after addition of dodecanethiol at room temperature.

Mere addition of the thiol to the as-prepared colloid itself induces many interesting changes (Figure 2). We no longer see the big polyhedral particles. Instead, the particles are broken apart to sizes varying from 2 to 6 nm.

(7) Schaff, T. G.; Knight, G.; Shafigullin, M. N.; Bor, R. F.; Whetten, R. L. *J. Phys. Chem. B* **1998**, *102*, 10643.

(8) Borohydride reduction of $AuCl_3$ in a 0.35 M DDAB micelle solution leads to a fairly monodisperse colloid. See: Lin, X. M.; Sorensen, C. M.; Klabunde, K. J. *Chem. Mater.* **1999**, *11*, 198. However, taking a 0.02 M DDAB micelle solution makes the as-prepared gold colloid highly polydisperse.

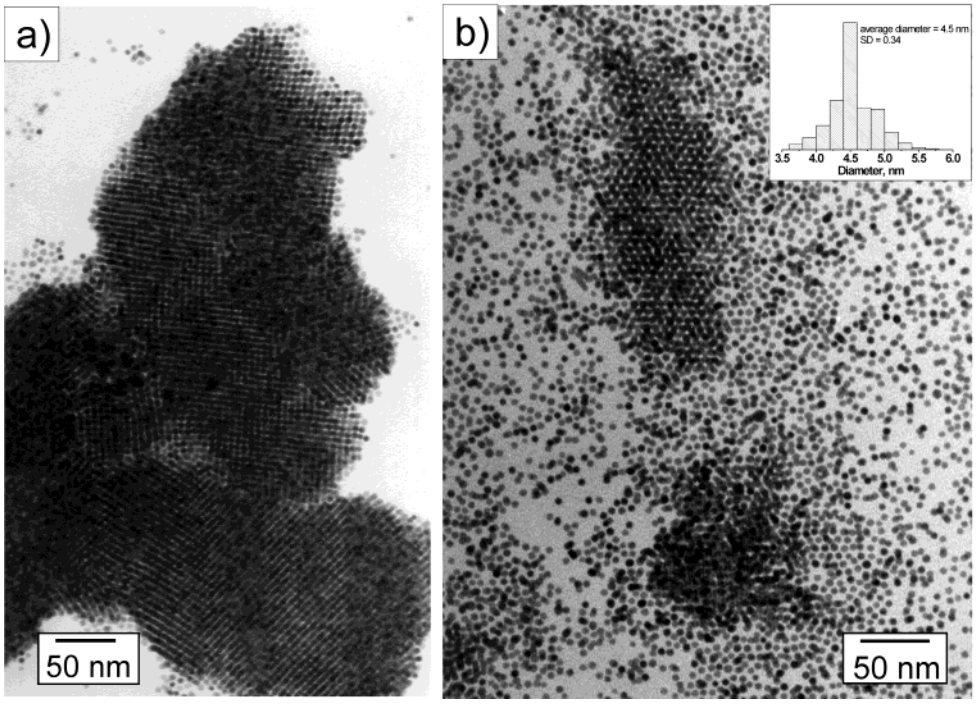

Figure 3. (a) TEM image of the gold colloid after digestive ripening with octanethiol showing the 3D superlattices. (b) TEM image of a hot and diluted Au−C_8SH colloid depicting the separate particles. The inset in (b) shows the particle size distribution.

Obviously, these changes are brought upon by the addition of thiol. It has been observed in the high-resolution TEM images that the as-prepared particles (before thiol addition) have many cleavage planes and grain boundaries.[9] We speculate that addition of excess thiol (Au/thiol = 1:30), which now replaces the DDAB as the stabilizing agent, transforms the big particles into narrower size distributed particles by attacking the big particles through sites where DDAB is not present. Also, the cleavage planes and grain boundaries might allow the thiol to reach the interior portions of the big particles and break them into smaller particles. The thiols used in these experiments have much lower volumes compared to that of DDAB, which might explain the stabilization of smaller particles upon their addition.

The next step in our synthetic procedure is the digestive ripening. We do not see any significant dependence of the particle size or morphology of the aggregates on the alkyl chain length (C_8, C_{10}, C_{12}, or C_{16}) of the thiol when they were first added to the as-prepared colloid. However, refluxing leads to dramatic changes depending on the chain length, and these are discussed in detail below.

All the colloids look very red in color while they are under reflux conditions at $T \approx 120$ °C. The differences among them become visible when the colloids are cooled to room temperature ($T \approx 23$ °C). The Au−C_8SH colloid completely settles down to the bottom of the vial with a clear, colorless supernatant. Au−C_{10}SH and Au−C_{12}SH look very similar to each other with a purple precipitate at the bottom of the vial in both cases. The supernatant is pale pink in Au−C_{10}SH and darker in Au−C_{12}SH. There is no or very little precipitate in the Au−C_{16}SH case, and the colloid remains a very intense red. These results suggest that at high temperatures, $T \geq 80$ °C, all the colloids are stable, that is, soluble in toluene; but at room temperature, their tendency to form superlattices and precipitate increases with decreasing alkyl chain length of the thiol.

(9) Stoeva, S. I. et al., Unpublished results.

Figures 3−6 depict the TEM images observed for the different colloids which were cast on the TEM grids after vigorous shaking. As can be clearly seen from the TEM images, the alkyl chain length of the thiol used crucially decides the morphology of the superlattices of the gold nanocrystals. Namely, Au−C_8SH leads to only 3D ordering, while both 3D and 2D ordered arrays are present in the Au−C_{10}SH and Au−C_{12}SH cases and Au−C_{16}SH forms exclusively 2D layers. (The TEM image in Figure 3b was taken from a hot and very dilute Au−C_8SH colloid so as to separate the particles well and determine the particle size distribution.) The propensity to form 3D lattices and their sizes are usually greater in the Au−C_8SH and Au−C_{10}SH cases compared to Au−C_{12}SH. The majority of Au−C_{16}SH colloid forms only 2D monolayers (Figure 6). We did not see many 3D ordered structures in the Au−C_{16}SH colloid. In the few places we found multilayers, there was no order, and it was probably caused by some defect in the grid or due to the wetting and drying nature of the excess thiol present in the colloidal solution.

The average particle size increases from 4.5 to 5.5 nm as we change the digestive ripening ligand from C_8SH to C_{16}SH. It has been reported that the dependence of particle size on the thiol chain length is nonmonotonic, with a maximum cluster size for C_{10}SH, the reasons for which are not very clear.[3b] However, a general explanation offered is that there is an optimum size for the particles that allows the most stable packing of the capped organic ligands. On this basis, the lengthier ligands should prefer less curved surfaces favoring larger sized particles as we change the capped ligand from C_8SH to C_{16}SH. However, a complete explanation must await further work.

The optical spectral results of the vigorously shaken colloids, at room temperature, are in complete agreement with the TEM observations and are given in Figure 7. The optical spectrum of the as-prepared colloid shows a broad peak with a peak maximum around 530 nm attributed to the excitation of plasma resonances or interband transi-

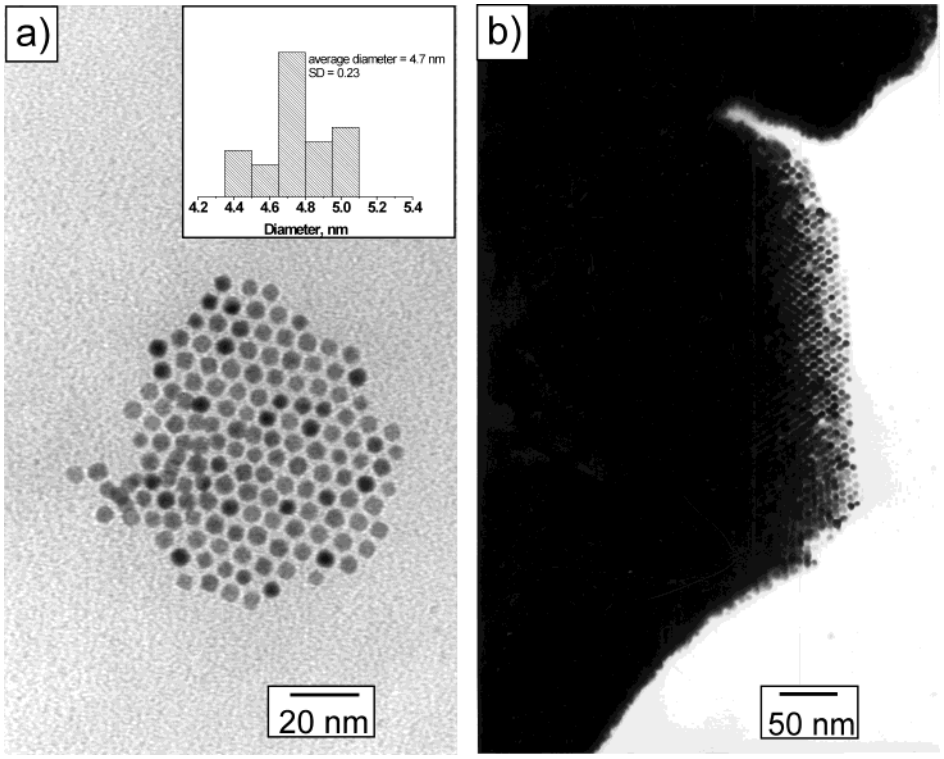

Figure 4. TEM image of the gold colloid digestive ripened by decanethiol depicting the monolayers (a) and ordered superlattices (b). The inset in (a) displays the particle size distribution.

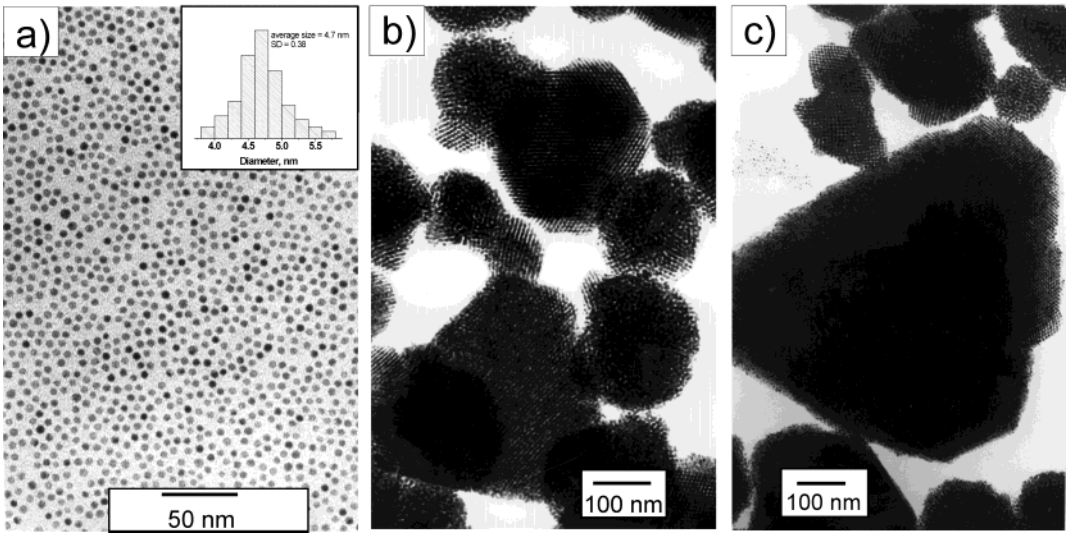

Figure 5. TEM images of the gold colloid after digestive ripening with dodecanethiol. The monolayers (a) and the 3D ordered lattices (b,c) are clearly seen. The particle size distribution is given in the inset of (a).

tions.[10] The plasmon band could also be seen for Au−C_8SH and Au−C_{10}SH apart from a large tail above 700 nm. For Au−C_{12}SH, we can see a shoulder centered at 620 nm accompanying the 530 nm peak. Au−C_{16}SH reveals only the gold plasmon peak. It is well documented now that the optical properties of gold colloids are highly dependent on the level of particle aggregation, interparticle separation, and particle sizes.[11] Thus the large tail observed for Au−C_8SH and Au−C_{10}SH illustrates that the particles are forming aggregates in solution which supports the TEM findings (Figure 3 and Figure 4). When gold nanoparticles self-assemble into a 3D superlattice, there is an increase in the dielectric constant of the medium, shifting the plasmon peak to lower energies.[3,11,12] The superlattices are bigger, and the ligand chain length separating the particles is smaller for Au−C_8SH and Au−C_{10}SH, making the electromagnetic coupling between the particles stronger and resulting in the larger shifts. As far as we are aware, this is the first instance where such large shifts of the plasmon peak for gold superlattices with particle sizes of 5−6 nm are observed. We found only one other report where such large shifts into the near-

(10) Mie, G. *Ann. Phys.* **1908**, *25*, 377.

(11) (a) Taleb, A.; Petit, C.; Pileni, M. P. *J. Phys. Chem. B* **1998**, *102*, 2214. (b) Storhoff, J. J.; Lazarides, A. A.; Mucic, R. C.; Mirkin, C. A.; Letsinger, R. L.; Schatz, G. C. *J. Am. Chem. Soc.* **2000**, *122*, 4640.

(12) (a) Quinten, M.; Kreibig, U. *Surf. Sci.* **1986**, *172*, 557. (b) Creighton, J. A.; Eadon, D. G. *J. Chem. Soc., Faraday Trans.* **1991**, *87*, 3881. (c) Link, S.; El-sayed, M. A. *J. Phys. Chem. B* **1999**, *103*, 4212. (d) Lazarides, A. A.; Schatz, G. C. *J. Chem. Phys.* **2000**, *112*, 2987. (e) Lazarides, A. A.; Schatz, G. C. *J. Phys. Chem. B* **2000**, *104*, 460.

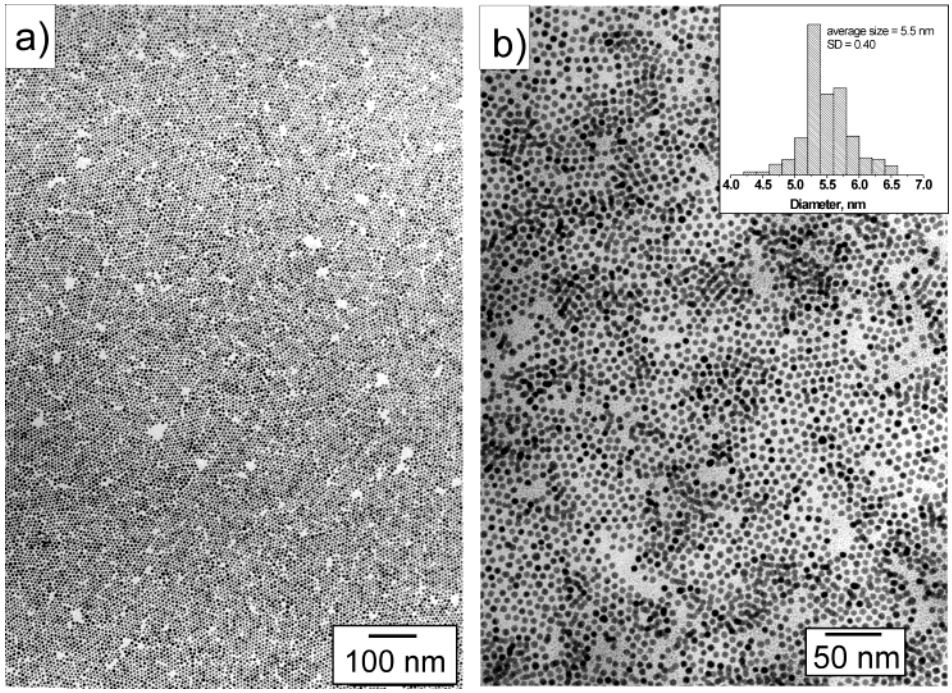

Figure 6. TEM image of the gold colloid after digestive ripening with hexadecanethiol where (a) and (b) were taken from samples prepared from different batches. The inset in (b) shows the particle size distribution.

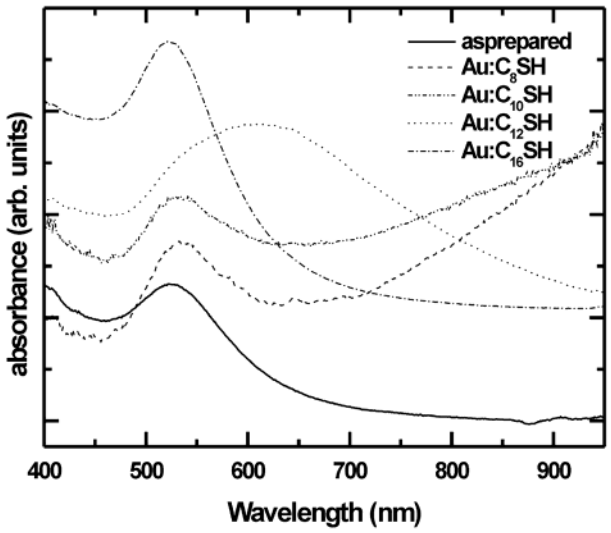

Figure 7. Room-temperature optical spectra of the as-prepared gold colloid and those digestive-ripened by different alkanethiols.

infrared regions were mentioned for arrays of gold particles albeit with particle sizes above 70 nm.[3] Most of the theoretical work on the optical properties of these colloids is also restricted to the visible region (400−900 nm).[12] Also, we observed a temperature dependence of these shifts for our colloids (vide infra). Further work is in progress in our group to completely understand the reasons for such large shifts.

For all practical purposes, the properties of the Au−C_{10}SH colloid are sandwiched between those of Au−C_8SH and Au−C_{12}SH. Precisely, it shows many 3D superlattices and very few regions of 2D monolayers (Figure 4). The size of the superlattices is generally smaller than that of Au−C_8SH but bigger than that of Au−C_{12}SH. The optical spectra of Au−C_{10}SH are more similar to those of Au−C_8SH than to those of Au−C_{12}SH, indicating that the optical properties are mainly controlled by the superlattices rather than the separate particles.

At room temperature, the Au−C_{12}SH colloid is a mixture of both precipitated 3D superlattices and dissolved separate particles, perhaps in equilibrium with each other. This could be concluded from the fact that there is some precipitate at the bottom of the vial and the supernatant still remains red. The precipitate is due to the superlattices which settle down to the bottom due to the gravitational forces, and the separate particles still remain suspended in solution. The TEM images clearly show many smaller 3D superlattices, and we could also observe several regions with monolayers of separate particles (Figure 5). In fact, when we have carefully taken a sample of the Au−C_{12}SH from the precipitate at bottom of the vial, the TEM images displayed only 3D superlattices and no monolayers could be detected. Predictably, the optical spectra of the Au−C_{12}SH colloid show the gold plasmon band at 530 nm with a shoulder ascribed to the superlattices at 620 nm. Here, the capping ligand is lengthier than C_8H_{17}SH and $C_{10}H_{23}$SH; as a result, the distance between the particles is larger and also the superlattices are not as big. Both of these factors yield a smaller shift of the plasmon peak.

The optical spectra of the Au−C_{16}SH are in complete agreement with the TEM results and support the arguments presented so far very well. They show only the gold plasmon band at 530 nm as expected from separate particles. The TEM image also shows only 2D monolayers albeit with very poor ordering (Figure 6). Probably the particles come together on the TEM grid while the solvent is being evaporated, unlike the other two cases where the superlattices are formed in the solution. However, the plasmon peak is very sharp compared to that of the as-prepared colloid due to the much narrower size distribution after digestive ripening.

To understand qualitatively the solubility features, we have calculated the van der Waals attraction potential

between the metal cores in all of the three cases, utilizing the equation shown below:[13]

$$V(D) = -\frac{A}{12}\left[\frac{R}{D[1 + D/2(R_A + R_B)]} + \frac{1}{1 + D/R + D^2/4R_AR_B} + 2\ln\left(\frac{D[1 + D/2(R_A + R_B)]}{R[1 + D/R + D^2/4R_AR_B]}\right)\right]$$

Here, A is the Hamaker constant which is equal to 1.95 eV for gold. R_A and R_B are the radii of the two spheres between which the attraction forces are to be calculated. (In our case $R_A = R_B$.) D is the gap between the nearest surfaces of adjacent spheres, and R is the reduced radius given by $2R_AR_B/(R_A+R_B)$. We have assumed that the two spheres are separated by the chain length of the thiol attached to the gold particles supposing that the two alkyl chains on two adjacent gold particles are fully interdigitated. This is justified since the average separation between the particles is found to be almost equivalent to the chain length of the thiol used although we could not exactly determine it owing to the thick superlattices formed. The attraction energies turn out to be $5k_BT$, $2.2k_BT$, $2k_BT$, and $0.6k_BT$ for Au−C_8SH, Au−C_{10}SH, Au−C_{12}SH, and Au−C_{16}SH, respectively, where k_B is the Boltzmann constant and $T = 300$ K. From these results, we can clearly expect Au−C_8SH, Au−C_{10}SH, and Au−C_{12}SH to favor aggregation since the attraction energies are 2−5 times larger than the room-temperature thermal energy, enabling them to overcome the solvation energies and room-temperature thermal vibrations. In Au−C_{16}SH, the attraction is smaller than the room-temperature thermal energy and hence it, along with solvation energies, forces them to be separate particles. Although these empirical calculations qualitatively support our results, we cannot rule out other possibilities. It is established that among the alkylthiols, dodecanethiol is strongly bound to the gold surface compared to hexanethiol or hexadecanethiol.[3b] In our case, the increased lability of hexadecanethiol compared to the other three thiols might be resulting in the formation of weakly bound multilayers on the gold surface hindering the development of 3D superlattices.

If these superlattices are assumed to be similar to the normal "molecular" crystals, then it should be possible to make these superlattices more soluble with a change of temperature. Indeed, the optical spectra of the three colloids prepared in this study at 80 °C exhibit only the gold plasmon band in all the four cases (Figure 8). The large tail noticed for Au−C_8SH and Au−C_{10}SH and the shoulder observed for Au−C_{12}SH have disappeared completely, suggesting that the superlattices are now broken apart. It was also seen that the color of all the colloids was similar at these elevated temperatures. It generally takes a few minutes to several hours for the tails and shoulders, credited to superlattices, to reappear fully when the samples are cooled to room temperature. This suggests that the self-organization of the gold colloids into superlattices is a very slow but reversible phenomenon. The kinetics involved in the "crystallization" of these nanoparticles might be more complex than that of normal molecular solids, hence the delay in returning to the original state. Nevertheless, the superlattices of the gold nanoparticles overall have a very similar behavior to that of normal crystalline compounds.

(13) (a) Hamaker, H. C. *Physica* (*Utrecht*) **1937**, *4*, 1058. (b) Ohara, P. C.; Leff, D. V.; Heath, J. R.; Gelbart, W. M. *Phys. Rev. Lett.* **1995**, *75*, 3466.

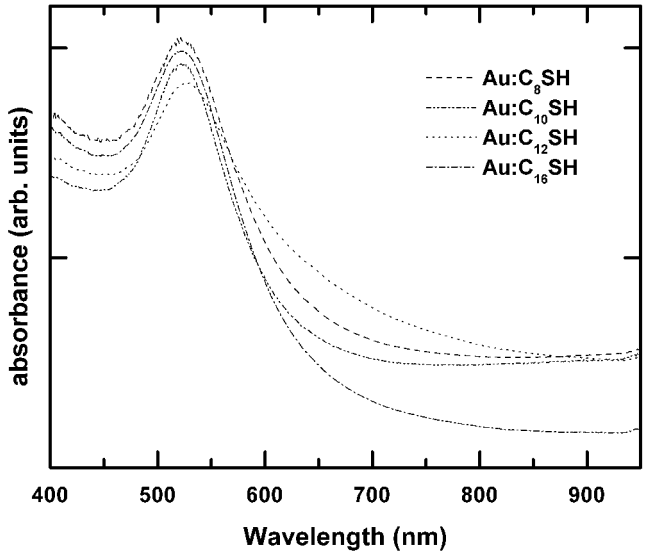

Figure 8. High-temperature optical spectra of gold colloids digestive-ripened by different alkanethiols.

Conclusions

The convenience and effectiveness of the digestive ripening method in converting a highly polydisperse gold colloid into a very monodisperse one using several thiols is presented. Altering the interparticle separation of the gold nanoparticles through the alkyl chain length critically controls their solubility behavior and also leads to the formation of exclusive 2D or 3D superlattices or a combination of them. The stronger and larger 3D superlattices observed for the Au−octanethiol and Au−decanethiol cases also lead to large shifts of the optical spectra into the near-infrared region. This is the first instance where such large shifts in the optical spectra for 5−6 nm particles are observed. The tendency to form separate particles with longer chain length (C_{16}) thiols and to aggregate into 3D superlattices with short chain length (C_8 and C_{10}) thiols is rationalized from the decrease in particle−particle attraction energies as the thiol chain length is increased. The fact that these superlattices have similar solubility behaviors to those of normal molecular solids is very encouraging. This might enable us to separate a macroscopic "nanosupercrystal" so as to study its physical properties such as melting point and so forth, and we have already made significant progress toward this goal. It is also of great interest to understand the mechanistic aspects of the digestive ripening procedure and to see whether this method would be applicable to other metals such as silver, and efforts are currently under way in our lab in this direction.

Acknowledgment. We gratefully acknowledge the financial support from the National Aeronautics and Space Administration (NASA). We thank the Kansas State University Biology Research Microscope and Image Processing Facility, which has been supported in part by the NSF EPSCoR Program, by the NASA EPSCoR Program, by University resources, and by the Kansas Agricultural Experiment Station.

LA020181D